

Femtosecond Photo-Induced Multiphoton Analog Computation for Symmetry-Based Pattern Classification

Lev Chuntonov, Leonid Rybak, Andrey Gandoman, and Zohar Amitay

Schulich Faculty of Chemistry, Technion – Israel Institute of Technology, Haifa 32000, Israel

Abstract

Multiphoton femtosecond coherent control is used for implementing innovative photo-induced analog coherent computation that generally might be a basis for future "smart hardware". The specific implemented computational task is the classification of an unknown sequence into one of the three groups: (i) a constant sequence that is composed of identical numbers, (ii) a sequence that is antisymmetric around a given point, or (iii) neither. The input sequence is encoded into the spectral phases of a broadband femtosecond pulse and the computational task is being carried out by the multiphoton nonlinear response of the irradiated physical system. Here, it is the simultaneous coherent two- and three-photon absorption in atomic sodium (Na). The corresponding computational resources are the manifold of initial-to-final multiphoton excitation pathways photo-induced by the broad spectrum of the irradiating femtosecond pulse. The answer is obtained by measuring only two observables, which are two state-populations excited via the two- and three-photon absorption processes. Hence, the computational task is accomplished in a constant number of operations irrespective of the sequence length. As such, the presented scheme, where the femtosecond pulse serves as a query and the irradiated physical system serves as an oracle, provides a sufficient gain in the computational complexity.

PACS numbers: 32.80.Qk, 42.50.Ex

Electronic address: amitayz@tx.technion.ac.il

Analog quantum computation (AQC) utilizes the similarity between the formal mathematical description of the physical phenomena and the formulation of the problem being solved. The information is processed by exploiting the physical phenomena directly: it is the system evolution that processes the information and performs a computational task [1, 2, 3]. AQC is aimed to solve otherwise intractable problems, once the similarity is found between the mutual relations of the problem parameters and the corresponding physical quantities of the system [3, 4, 5, 6, 7, 8, 9, 10, 11]. Here we exploit the femtosecond coherent control [12, 13, 14, 15, 16, 17] of multiphoton absorption to perform a specific computational task: classification of the unknown sequence into the three groups: a sequence composed of the identical components, a sequence that is antisymmetric about a specific point, or neither. The concept of using the femtosecond pulse as a query and an excited system as an oracle provides a sufficient gain in the computational complexity. The experimentally demonstrated approach requires only two measurements to accomplish the computational task irrespectively of the sequence length.

Following from their coherence over a broadband spectrum, femtosecond pulses are used as a unique tool for coherent control and coherent spectroscopy of matter [16, 17, 18, 19, 20, 21, 22]. The broadband spectrum provides a variety of photoinduced pathways that are used for the multiphoton excitation. All of the such pathways interfere between them and contribute to the finally excited amplitude: constructive interference enhances the excited amplitude, while destructive interference suppresses it. The recently developed pulse-shaping techniques [23, 24, 25] enables access to the parameters of different frequency components of the pulse independently. Among the parameters that could be adjusted are phase, amplitude, and polarization of the frequency components. Control over these parameters is directly translated to the control over the interference between the photoinduced pathways and, hence, to the control over the excited amplitude.

The basic idea of the presented here experiments is to use the interference pathways of the multiphoton excitation as the computational and information processing tool. The unknown information to be processed is translated into the transformation $\hat{U} = \exp[i \phi(\omega)]$ which is applied to the electric field of the excitation femtosecond pulse with spectral amplitude $E(\omega)$. This transformation results in a shaped pulse $E(\omega) \exp[i \phi(\omega)]$, where $\phi(\omega)$ is a spectral phase of frequency ω . The phase associated with each multiphoton pathway is equal to the sum of the phases of all the involved photons. All the possible combinations

of the excitation pathways provided by the shaped pulse interfere together during the excitation, i.e. evaluated at a single event, as opposed to the classical information processing, where each information component is evaluated separately. After the excitation, the resulted excited amplitude contains the information on the nature of the interference. Relying on the knowledge of the light-matter interaction mechanism, measurement of the excited amplitude can characterize the information originally used to shape the excitation pulse. Different physical systems respond in a different way to the excitation with a given pulse shape. This is why the system used for the processing should be carefully chosen to suit the specific computational task. It is a general and very important attribute of AQC – its inherent problem-specific nature: one should always find a physical system with quantities which mutual relation corresponds to these of the problem to solve.

The computational task that we consider is a classification of the unknown sequence into the three groups: a sequence composed of the identical components, which is referred as constant sequence, a sequence that is antisymmetric about a specific point – antisymmetric sequence, or neither, referred as random. For that purpose we encode the subjected sequences into the phase patterns const , antisym , and random of the broadband spectrum. Each component of the sequence is translated into the phase magnitude of the corresponding frequency using the pulse shaping technique. The physical process that suits the computational needs is the two-channel femtosecond multiphoton absorption. In the proposed scenario the amplitudes of the excitation channels characterize the type of the sequence encoded into the transformation \hat{U} . The different response by the different channels to the applied transformation is a key property of the system that solves the presented classification task.

One of the excitation channels exploited for our computational task is a non-resonant two-photon absorption channel [18, 19]. The excited amplitude in this case is proportional to $A^{(2)}(\omega) = \frac{R+1}{1} E(\omega=2\omega_0)E(\omega=2\omega_0+\omega_d)$. It interferes all the possible two-photon pathways with transition frequency ω , each such pathway is composed of two photons with frequencies $\omega=2\omega_0$ and $\omega=2\omega_0+\omega_d$, i.e., two frequencies located symmetrically around $\omega=2\omega_0$. The phase associated with each pathway is $\phi(\omega=2\omega_0) + \phi(\omega=2\omega_0+\omega_d)$. For the transform-limited (TL) pulse, which is the shortest pulse for a given spectrum, $\phi(\omega) = 0$ and all the excitation pathways interfere constructively. The same applies to the transformations corresponding to the constant sequences \hat{U}^{const} with $\phi(\omega) = \text{const}$ as they add only a global phase factor,

identical to all the interfering pathways. The two-photon non-resonant channel is also invariant to the transformations corresponding to the antisymmetric sequences \hat{U}^{antisym} , while the point of the inversion corresponds to half the two-photon transition frequency $\omega = 2$. For that case $(\omega = 2) = (\omega = 2 + \dots)$ holds, and all the available pathways obtain zero relative phase. Hence, the application of \hat{U}^{antisym} implies constructive interference between all the pathways. On the other hand, along any other possible channel without special sensitivity to the symmetry of the transformation, the induced excitation pathways interfere destructively. Such channel is not invariant to \hat{U}^{antisym} , but to \hat{U}^{const} .

Combining all the described here together, we build a truth table for the sequence classification: constant sequences induce fully constructive interference along both channels and they are associated with a maximal amplitude of both excitation channels, which is actually the same as for the TL pulse. The antisymmetric sequences are associated with fully constructive interference along the two-photon non-resonant channel, and with destructive interference along the channel without any symmetrical properties. The random sequences induce destructive interference along both channels and the excited amplitude by the corresponding shaped pulses is sufficiently less than by the TL pulse. To demonstrate this idea experimentally, we have chosen atomic two-channel system, which includes non-resonant two-photon absorption channel coherently incorporated within a resonant-mediated (2+1) three-photon absorption channel.

The two-channel excitation considered here is shown schematically in Fig. 1. It involves an initial ground state $|g\rangle$ and two excited states $|f_1\rangle$ and $|f_2\rangle$. The $|g\rangle$ and $|f_1\rangle$ states are coupled by a non-resonant two-photon coupling provided by a manifold of states $|j\rangle$ that are far from resonance, while the $|f_1\rangle$ and $|f_2\rangle$ states are coupled resonantly by one-photon coupling. Hence, when irradiated with a weak (shaped) femtosecond pulse of temporal electric field $E(t)$, two multiphoton absorption channels are induced simultaneously: a non-resonant two-photon absorption channel from $|g\rangle$ to $|f_1\rangle$ is induced simultaneously with a resonance-mediated (2+1) three-photon absorption channel from $|g\rangle$ to $|f_2\rangle$ with $|f_1\rangle$ as an intermediate state. The amplitude of the latter channel is determined by both intra-group and inter-group interferences corresponding to on-resonant and near-resonant with $|f_1\rangle$ state three-photon excitation pathways respectively. The pathways induced by the pulse shaped with \hat{U}^{antisym} interfere destructively along this channel. Although the TL pulse and, hence, the shaped pulses corresponding to \hat{U}^{const} do not induce the maximal constructive

interference for the (2+1) resonance-mediated channel, the pulse should be shaped in a very special way to enhance the amplitude excited by the TL pulse [20, 21, 22]. This is not the case of the present experiment.

Alternatively, another two-photon non-resonant channel can be chosen for that purpose with different transition frequency $\omega_{ch_1} \neq \omega_{ch_2}$. Obviously, while the channel 1 is sensitive to the sequences antisymmetric about $\omega_{ch_1}=2$, the channel 2 is sensitive to the antisymmetric sequence with the inversion point at $\omega_{ch_2}=2$. The corresponding physical system is a second harmonic crystal, with each frequency of the produced harmonics being a different excitation channel measured separately. The choice of such a crystal provides a wide tunability upon the point of antisymmetric inversion of the sequences to be checked, while the sensitivity to this specific point (the precision of the classification) in this case is set by the resolution of the detection system. In the atomic case, this sensitivity is extremely high due to the narrow width of the atomic lines.

Suppose now that unknown sequence $f(x)$ is optically encoded into the phase pattern $\phi(x)$ of the pulse using a pulse shaping technique. We check whether there is an inversion point x_0 corresponding to the frequency of the non-resonant two-photon transition $\omega_{fg}=2 = \omega_{f_1g} + \omega_{f_2g}$. The processing of the information is done upon the excitation of the atomic system with the shaped pulse from its ground state $|g\rangle$ to the excited states $|f_1\rangle$ and $|f_2\rangle$. The population of the excited states P_{f_1} and P_{f_2} is used as a readout channel and compared with the population excited by the TL pulse. If $P_{f_1;f}(x) = P_{f_1;TL}$ and $P_{f_2;f}(x) = P_{f_2;TL}$, the pulse spectral phase is a constant pattern which represents encoded sequence $f(x) = \text{const.}$ If $P_{f_1;f}(x) = P_{f_1;TL}$, but $P_{f_2;f}(x) \neq P_{f_2;TL}$, the pulse spectral phase is antisymmetric about ω_{fg} the encoded sequence satisfies $f(x_0 - \Delta) = f(x_0 + \Delta)$. If $P_{f_1;f}(x) \neq P_{f_1;TL}$ and $P_{f_2;f}(x) \neq P_{f_2;TL}$, the corresponding phase pattern is neither antisymmetric nor constant and is referred here as random. Overall, the computational task is performed by comparing the outcome of the two specific measurements only, irrespectively of the length of sequence to be classified.

The physical model system of the study is the sodium (Na) atom [26], with the 3s ground state as $|g\rangle$, the 4s state as $|f_1\rangle$, and the 7p state as $|f_2\rangle$ (see Fig. 1). The transition frequency $\omega_{f_1g} = \omega_{4s;3s} = 25740 \text{ cm}^{-1}$ corresponds to two 777-nm photons and the transition frequency $\omega_{f_2g} = \omega_{7p;4s} = 12801 \text{ cm}^{-1}$ corresponds to a 781.2-nm photon. The 3s-4s non-resonant two-photon coupling originates from the manifold of p-states, particularly from the 3p state [$\omega_{3p;3s} = 16978 \text{ cm}^{-1}$ (589 nm)]. The sodium is irradiated with phase-shaped linearly-

polarized femtosecond pulses having a Gaussian intensity spectrum centered around 780 nm (12821 cm^{-1}) with 5.8-nm (95 cm^{-1}) bandwidth (180-fs TL duration).

Experimentally, a sodium vapor in a heated cell is irradiated with such laser pulses, after they undergo shaping in an optical setup incorporating a pixelated liquid-crystal spatial light phase modulator [23]. The effective spectral shaping resolution is $\Delta_{\text{shaping}} = 2.05 \text{ cm}^{-1}$ (0.125 nm) per pixel. The peak intensity of the TL pulse is below 10^9 W/cm^2 . Following the interaction with a pulse, the population excited to the 4s state radiatively decays to the lower 3p state, which then decays to the 3s ground state. The 3p-3s fluorescence serves as the relative measure for the total 4s population $P_{f_1} = P_{4s}$. The population excited to the 7p state undergoes radiative and collisional decay to lower excited states, including the 4d, 5d, 6d, and 6s states. The fluorescence emitted in their decay to the 3p state serves as the relative measure for the total 7p population $P_{f_2} = P_{7p}$. The fluorescence is measured using a spectrometer coupled to a time-gated camera system. The 3p-3s fluorescence part originating from the 4s state is discriminated from the part originating from the 7p state by using a proper detection gate width, utilizing the different time scales of the 4s-to-3p and 7p-to-3p decays.

Fig. 2 presents experimental results measured for the randomly generated 20,000 sequences encoded into the phase patterns. Half of the sequences are urged to be antisymmetric about $\Delta_{4s;3s}$. Each pattern is composed of 26 bins which can obtain values randomized in the $[-2; 2]$ interval. On Fig. 2 panel (a) presented a two-dimensional histogram of the measured population: x-axis represents the population of 4s state, y-axis represents the population of 7p state. The color code and the topological curves represent the occurrence of phase patterns with the corresponding signal. All the results presented here are given relative to the absorption induced by the transform-limited (TL) pulse. For convenience, we introduce the TL-normalized absorption measures $\mathbb{P}_{f_1} = P_{f_1}/P_{f_1,TL}$ and $\mathbb{P}_{f_2} = P_{f_2}/P_{f_2,TL}$. The three regions, corresponding to the constant, antisymmetric, and random phase patterns are clearly distinguished on the histogram. The region with the peak at $(\mathbb{P}_{4s}=1, \mathbb{P}_{7p}=0.5)$ correspond to the antisymmetric sequences, encoded to the phase patterns, while the region with the peak at $(\mathbb{P}_{4s}=0.25, \mathbb{P}_{7p}=0.25)$ correspond to the random sequences. The region with the peak at $(\mathbb{P}_{4s}=1, \mathbb{P}_{7p}=1)$ correspond to the constant sequences with the populations identical to the TL pulse. The broadening of that peak directly reflects the signal-to-noise experimental ratio. As seen from the figure, the measured population, corresponding to the

sequence encoded to the phase pattern of the excitation pulse can be used for the classification of the sequence by its properties, based on the presented above truth table.

On Fig. 2 panels (b) and (c) we draw the projections of the two-dimensional histogram of panel (a) on the 7p and 4s population axis. As seen from panel (c), the 4s population signal clearly distinguish between the random sequences and the rest: 100% of the random sequences produce signal less than the corresponding TL pulse. However, this signal does not distinguish between the constant and antisymmetric sequences. The latter is done by analyzing the 7p population signal [see panel (b)]. For the detailed analysis of the distribution we plot the cumulative sum function corresponding to the antisymmetric sequences in dashed black line and obtain that 96% of the sequences produces 7p population signal less than the corresponding TL pulse. It means that the experimental false identification of antisymmetric sequence as a constant one or vice versa is below 4%. This value can be improved by improving the signal-to-noise ratio.

We have checked the sensitivity of the method by shifting the phase pattern center of symmetry by one pixel apart from $\omega_{4s,3s}$. The corresponding results are shown on Fig. 2 panel (b). The distribution of the antisymmetric patterns is moved from the region of $P_{4s} = 1$ to the region corresponding to random patterns. The reason for the high sensitivity of the signal to the exact location of the inversion point is in the very narrow nature of the atomic resonance. While the phase pattern is antisymmetric about $\omega_{4s,3s} = 2$ it induces completely constructive interference of all the photoinduced pathways to the $|4s\rangle$ state. When the inversion point is shifted by δ , the maximally constructive interference would be induced for the state corresponding to the frequency $\omega_{4s,3s} + \delta$. In our experiment we have shifted the pattern by $\delta = \omega_{\text{shaping}} = 2.05 \text{ cm}^{-1}$. This shift was sufficient to reduce the constructive interference resulted in the reduced signal measured for that case.

To summarize, we have demonstrated an efficient solution to the unknown sequence classification problem. The classification is into three possible groups: a constant sequence, a sequence that is antisymmetric about specific point, and a random sequence. The sequences are encoded into the phases of the broadband femtosecond pulses. In the spirit of the analog quantum computation, the photoinduced dynamics of the excited atomic sodium is used to perform the computational task. The solution to the problem is obtained within the measurement of the two excitation channels irrespectively of the sequence length.

This research was supported by The Israel Science Foundation (grant No. 127/02), by

The James Franck Program in Laser Matter Interaction, and by The Technion's Fund for The Promotion of Research.

- [1] Feynman, R. P. Simulating physics with computers. *Int. J. Theor. Phys.* 21; 467-488 (1982).
- [2] Lloyd, S. Quantum information matters. *Science* 319; 1209-1211 (2008).
- [3] Brockett, R. W. A rational flow for the Toda lattice equations. in Helmke, U. et al. eds. *Operators, Systems, and Linear Algebra*, (B.G. Teubner, Stuttgart, 1997).
- [4] Farhi, E. et al. A quantum adiabatic evolution algorithm applied to random instances of an NP-complete problem. *Science* 292; 472-476 (2001).
- [5] Zak, M. Quantum analog computing. *Chaos Soliton. Fract.* 10; 1583-1620 (1999).
- [6] Zak, M. Quantum resonances for solving NP-complete problems by simulations. in Williams, C. P. ed. *Quantum Computing and Quantum Communications*, 160-166 (Springer-Verlag Berlin Heidelberg, 1999).
- [7] Weigert, S. Quantum diagonalization of Hermitian matrices. *J. Phys. A: Math. Gen.* 34; 5619-5624 (2001).
- [8] Georgoudas, I. G., Sirakoulis, G. Ch., & Andreadis, I. Modelling earthquake activity features using cellular automata. *Math. Comput. Model.* 46; 124-137 (2007).
- [9] Tokuda, E., Asahi, N., Yamada, T., Akazawa, M., & Amano, Y. Analog computation using single-electron circuits. *Analog Integr. Circ. S.* 24; 41-49 (2000).
- [10] Inokuchi, T., Yamada, T., Asai, T., & Amano, Y. Analog computation using quantum - ux parametron devices. *Physica C* 357 - 360; 1618-1321 (2001).
- [11] Bigourd, D., Chatel, B., Schleich, W. P., & Girard, B. Factorization of numbers with the temporal Talbot effect: optical implementation by a sequence of shaped ultrashort pulses. *Phys. Rev. Lett.* 100; 030202-1-4 (2008).
- [12] Tannor, D. J., Kosloff, R., & Rice, S. A. Coherent pulse sequence induced control of selectivity of reactions: Exact quantum mechanical calculations. *J. Chem. Phys.* 85; 5805-5820 (1986).
- [13] Shapiro, J. H., & Brumer, P. *Principles of the Quantum Control of Molecular Processes* (Wiley, New Jersey, 2003).
- [14] Warren, W. S., Rabitz, H., & Mahler, D. Coherent control of quantum dynamics: the dream is alive. *Science* 259; 1581-1589 (1993).

- [15] Rabitz, H., de Vivie-Riedle, R., Motzkus, M., & Kompa, K. Whither the future of controlling quantum phenomena? *Science* 288; 824-828 (2000).
- [16] Dantus, M. & Lozovoy, V.V. Experimental coherent laser control of physicochemical processes. *Chem. Rev.* 104; 1813-1859 (2004).
- [17] Lozovoy, V.V. & Dantus, M. Systematic control of nonlinear optical processes using optimally shaped femtosecond pulses. *Chem Phys Chem* 6, 1970-2000 (2005).
- [18] Meshulach, D. & Silberberg, Y. Coherent quantum control of two-photon transitions by a femtosecond laser pulse. *Nature* 396; 239-242 (1998).
- [19] Meshulach, D., & Silberberg, Y. Coherent quantum control of multiphoton transitions by shaped ultrashort optical pulses. *Phys. Rev. A* 60; 1287-1292 (1999).
- [20] Gandon, A., Chuntsov, L., Rybak, L., & Amitay, Z. Coherent phase control of resonance-mediated (2+1) three-photon absorption. *Phys. Rev. A* 75; 031401-1-4 (R) (2007).
- [21] Gandon, A., Chuntsov, L., Rybak, L., & Amitay, Z. Pulse-bandwidth dependence of coherent phase control of resonance-mediated (2+1) three-photon absorption. *Phys. Rev. A* 76; 053419-1-9 (2007).
- [22] Amitay, Z., Gandon, A., Chuntsov, L., & Rybak, L. Multichannel Selective Femtosecond Coherent Control Based on Symmetry Properties. *Phys. Rev. Lett.* 100; 193002-1-4 (2008).
- [23] Weiner, A.M. Femtosecond pulse shaping using spatial light modulators. *Rev. Sci. Instr.* 71; 1929-1960 (2000).
- [24] Brixner, T. & Gerber, G. Femtosecond polarization pulse shaping. *Opt. Lett.* 26; 557-559 (2001).
- [25] Brixner, T., Krampert, G., Niklaus P., & Gerber, G. Generation and characterization of polarization-shaped femtosecond laser pulses. *Appl. Phys. B* 74, S133-S144 (2002).
- [26] NIST Atomic Spectra Database (NIST, Gaithersburg, MD) available at <http://physics.nist.gov/asd>.

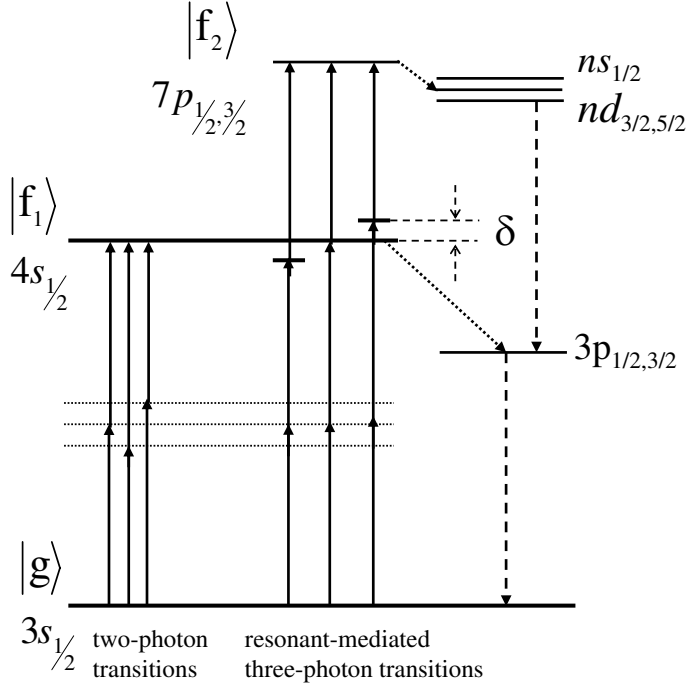


FIG. 1: The two-channel femtosecond excitation scheme of Na, including a non-resonant two-photon absorption channel from $|g\rangle$ $3s$ to $|f_1\rangle$ $4s$ and a resonance-mediated $(2+1)$ three-photon absorption channel from $|g\rangle$ $3s$ to $|f_2\rangle$ $7p$ via $|f_1\rangle$ $4s$. Shown in solid lines are examples of two- and three-photon pathways. The latter are either on resonance or near resonance with $|f_1\rangle$ (with detuning δ). The decay to the lower excited states is shown by dotted lines, the measured radiative decay indicating the population of the $7p$ and $4s$ states is shown by dashed lines.

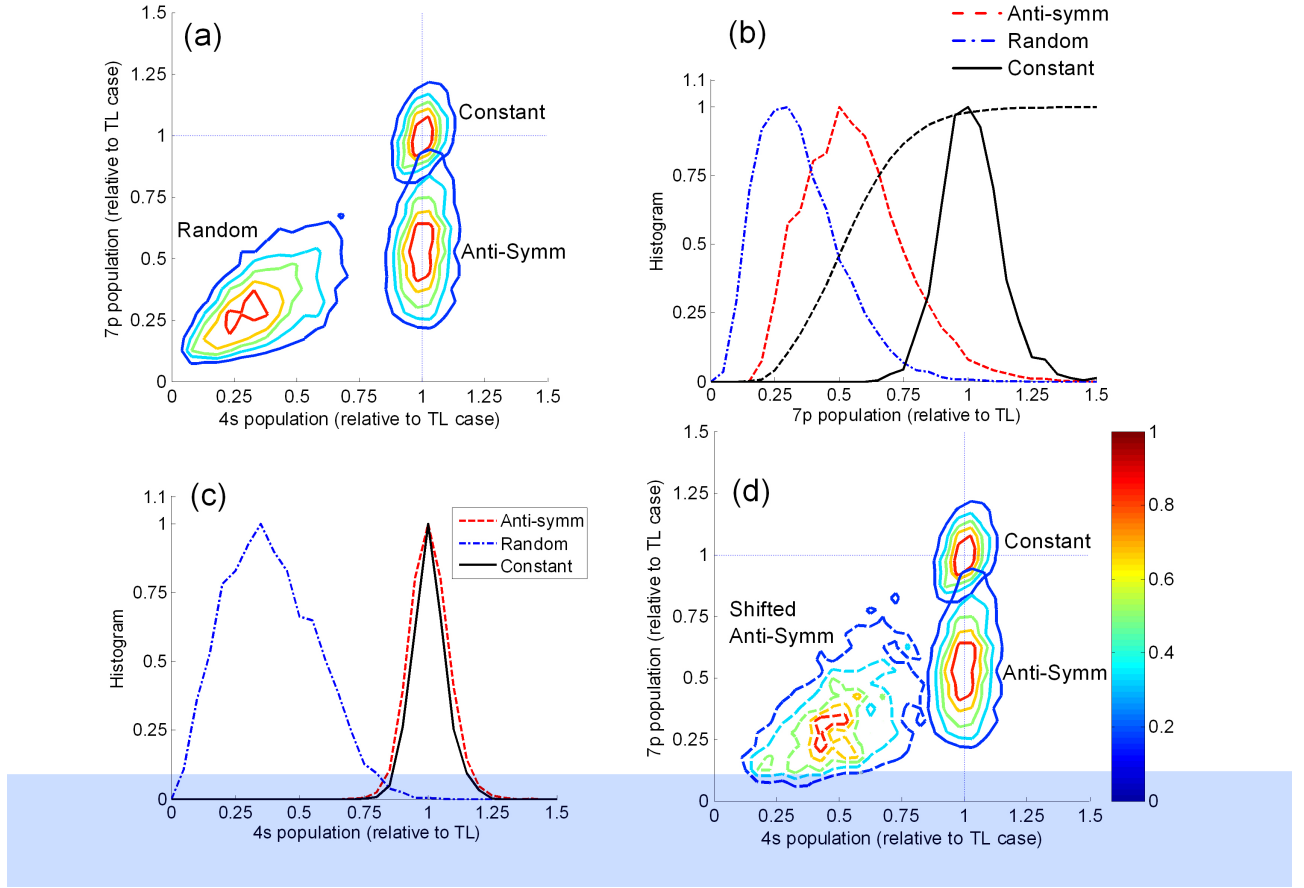


FIG .2: Experimental results for the 20,000 sequences encoded to the phase patterns of the shaped pulses. Each pattern has 26 bins with the values randomly generated within the interval of $[-1; 1]$. Half of the sequences were urged to be antisymmetric about $\pi_{4s,3s}$. Panel (a): Presented is two-dimensional histogram of the normalized to the unshaped (TL) pulse populations of 4s and 7p states. Three regions corresponding to the constant, antisymmetric, and random sequences are clearly distinguished. Panel (b): Projections of the panel (a) histogram on the axis of 7p population. Dashed black line indicates the cumulative sum of antisymmetric sequences histogram. At $(x = 1)$ it obtains the value of 0.96. Panel (c): Projections of the panel (a) histogram on the 4s population axis. Panel (d): Two-dimensional histogram of antisymmetric sequences shifted by $\pi_{4s,3s} = \pi_{\text{shaping}}$ from the original center of antisymmetry $\pi_{4s,3s} = 2$. The resulted sufficient shift of the distribution indicates the high sensitivity of the proposed method.